ENVIRONMENTAL RESEARCH
LETTERS

LETTER • OPEN ACCESS

Earth system responses to carbon dioxide removal as exemplified by ocean alkalinity enhancement: tradeoffs and lags

To cite this article: Aurich Jeltsch-Thömmes *et al* 2024 *Environ. Res. Lett.* **19** 054054

ENVIRONMENTAL RESEARCH
LETTERS

LETTER

Earth system responses to carbon dioxide removal as exemplified by ocean alkalinity enhancement: tradeoffs and lags

Aurich Jeltsch-Thömmes[1,*], **Giang Tran**[2], **Sebastian Lienert**[1], **David P Keller**[2], **Andreas Oschlies**[2] and **Fortunat Joos**[1]

[1] Climate and Environmental Physics and Oeschger Centre for Climate Change Research, University of Bern, Bern, Switzerland
[2] GEOMAR Helmholtz Centre for Ocean Research Kiel, Kiel, Germany
[*] Author to whom any correspondence should be addressed.

E-mail: aurich.jeltsch-thoemmes@unibe.ch

Keywords: carbon dioxide removal, ocean alkalinity enhancement, climate–carbon cycle projections

Supplementary material for this article is available online

OPEN ACCESS

RECEIVED
25 October 2023

REVISED
15 March 2024

ACCEPTED FOR PUBLICATION
26 April 2024

PUBLISHED
7 May 2024

Abstract

Carbon dioxide removal (CDR) is discussed for offsetting residual greenhouse gas emissions or even reversing climate change. All emissions scenarios of the Intergovernmental Panel on Climate Change that meet the 'well below 2 °C' warming target of the Paris Agreement include CDR. Ocean alkalinity enhancement (OAE) may be one possible CDR where the carbon uptake of the ocean is increased by artificial alkalinity addition. Here, we investigate the effect of OAE on modelled carbon reservoirs and fluxes in two observationally-constrained large perturbed parameter ensembles. OAE is assumed to be technically successful and deployed as an additional CDR in the SSP5-3.4 temperature overshoot scenario. Tradeoffs involving feedbacks with atmospheric CO_2 result in a low efficiency of an alkalinity-driven atmospheric CO_2 reduction of −0.35 [−0.37 to −0.33] mol C per mol alkalinity addition (skill-weighted mean and 68% c.i.). The realized atmospheric CO_2 reduction, and correspondingly the efficiency, is more than two times smaller than the direct alkalinity-driven enhancement of ocean uptake. The alkalinity-driven ocean carbon uptake is partly offset by the release of carbon from the land biosphere and a reduced ocean carbon sink in response to lowered atmospheric CO_2 under OAE. In a second step we use the Bern3D-LPX model in CO_2 peak-decline simulations to address hysteresis and temporal lags of surface air temperature change (ΔSAT) in an idealized scenario where ΔSAT increases to ~2 °C and then declines to ~1.5 °C as result of CDR. ΔSAT lags the decline in CO_2-forcing by 18 [14–22] years, depending close to linearly on the equilibrium climate sensitivity of the respective ensemble member. These tradeoffs and lags are an inherent feature of the Earth system response to changes in atmospheric CO_2 and will therefore be equally important for other CDR methods.

1. Introduction

Human-caused emissions of carbon dioxide and other agents cause global warming and dangerous anthropogenic interference in the Earth system (Siegenthaler and Oeschger 1978). Climate targets are designed to inform policies that would limit the magnitude and impacts of climate change caused by anthropogenic emissions of greenhouse gases and other substances. The Paris Agreement sets a target for the global mean air temperature to 'Holding the increase in the global average temperature to well below 2 °C above pre-industrial levels and pursuing efforts to limit the temperature increase to 1.5 °C above pre-industrial levels, recognizing that this would significantly reduce the risks and impacts of climate change.' (United Nations 2015).

Future emissions and concentration pathways toward meeting the Paris Agreement as well as other scenarios are typically developed with integrated assessment models (IAMs) (Riahi *et al* 2017, Rogelj

et al 2018). The IAM scenarios that are roughly compatible with the goals of the Paris Agreement all require in the first place the rapid and global-scale deployment of non-fossil energy production from renewable sources such as solar or wind. Additionally, these 'low' emissions pathways, such as SSP5-3.4-OS or SSP1-2.6, with a forcing ceiling of 3.4 and 2.6 Wm^{-2}, respectively, require the application of carbon dioxide removal (CDR) technologies (Smith *et al* 2016, Fuss *et al* 2018). Under CDR, CO_2 emissions are directly or indirectly removed from the atmosphere for long-term storage. Different CDR approaches have been proposed (see e.g. Smith *et al* 2016, Minx *et al* 2017, 2018, for an overview). Very roughly, these approaches can be split among the reservoir where the activity occurs: land-based, ocean-based, and direct air capture. A further distinction can be made between methods that seek to accelerate the uptake of atmospheric CO_2 by enhancing natural sinks and methods that seek to engineer the removal and subsequent storage of CO_2. An ocean-based approach that seeks to enhance a natural process called chemical weathering, which naturally removes up to 0.29 GtC yr^{-1} (Hartmann *et al* 2009), is ocean alkalinity enhancement (OAE, Ilyina *et al* 2013, González and Ilyina 2016, Caserini *et al* 2022), which is the addition of alkalinity to the surface ocean. This might be achieved by adding minerals (e.g. lime, limestone, olivine) or metal oxides to the ocean that dissolve in seawater. The increase in alkalinity then allows the ocean to absorb additional CO_2 from the atmosphere and permanently store it as bicarbonate or carbonate ions (Renforth and Henderson 2017, Campbell *et al* 2022), but there are significant barriers and uncertainties for effective OAE, e.g. related to scale (Köhler *et al* 2013), dissolution kinetics, and potential ecological impacts (Fakhraee *et al* 2023), as well as socio-economic concerns, e.g. public acceptance, governance, and costs (Cooley *et al* 2023).

An important question to address under CDR is how the Earth system in general, and its carbon inventories in particular, respond to CDR (Keller *et al* 2018a). The artificial direct removal of CO_2 from the atmosphere influences carbon fluxes between the atmosphere and land and ocean and leads to less carbon uptake than without CDR (Jeltsch-Thömmes *et al* 2020). Similarly, tradeoffs in carbon fluxes and inventories can also be expected under ocean- and land-based CDR approaches. Another question is related to inertia and (ir-)reversibility in the climate system (Frölicher and Joos 2010). For example, ocean deoxygenation and sea level rise continue for centuries to millennia after emissions stoppage (Clark *et al* 2016, Battaglia and Joos 2018, Oschlies 2021). Temperature and other parameters remain elevated for decades even after emissions have peaked and declined (Frölicher and Joos 2010, Boucher *et al* 2012, MacDougall 2013, Tokarska and Zickfeld 2015, Zickfeld *et al* 2016, Tokarska *et al* 2019, Jeltsch-Thömmes *et al* 2020, Schwinger *et al* 2022). It is therefore important to study and quantify inertia and hysteresis in the Earth system. Previous model studies have investigated various aspects of OAE in both CO_2-driven (e.g. Köhler *et al* 2013, Burt *et al* 2021, Wang *et al* 2023) and emission-driven simulations (e.g. Keller *et al* 2014, González and Ilyina 2016, Lenton *et al* 2018, Köhler 2020) and ranging from box-models (e.g. Köhler *et al* 2013) to highly-resolved regional ocean models (e.g. Wang *et al* 2023). Investigated aspects include questions related to regional vs. global OAE application and responses (e.g. González and Ilyina 2016, Lenton *et al* 2018, Burt *et al* 2021), dissolution of alkaline minerals and potential effects on marine biota (e.g. Köhler *et al* 2013, Fakhraee *et al* 2023), and OAE stoppage (e.g. Keller *et al* 2014). While some of the studies touch upon the partitioning of carbon between atmosphere, land, and ocean, to our knowledge no study has yet systematically investigated the tradeoffs in carbon storage between these carbon reservoirs and what it means for the efficiency (ε) of OAE to increase ocean carbon storage and to lower atmospheric CO_2. Further, to our knowledge large perturbed parameter ensemble studies investigating OAE have not yet been conducted and thus a knowledge gap about uncertainties remains.

Here, we apply ensembles of two Earth System Models of Intermediate Complexity, the Bern3D-LPX and the University of Victoria Earth System Climate Model (UVic-ESCM), in a probabilistic observation-constrained framework to investigate the effect of OAE on carbon fluxes and inventories and climate in the SSP5-3.4 overshoot scenario. SSP5-3.4 covers the main driver of global warming—fossil CO_2—and a wide range of other forcing agents and precursors with complex temporal evolution. This complexity may partly obscure forcing-response relationships. Therefore, we specifically investigate the timescales connected with the reversibility of surface air temperature (SAT) in an idealized CO_2-only overshoot scenario. We address the following questions:

(i) What is the trade-off in carbon storage between the atmosphere, ocean, and land under OAE and what does this mean for the efficiencies (ε) of OAE to increase ocean carbon storage and to lower atmospheric CO_2?
(ii) What is the role of Earth system inertia in CO_2-forcing overshoot (peak-decline) scenarios? How long does it take for global-mean SAT to return to the value passed under increasing forcing?

2. Methods

2.1. Models

Bern3D-LPX model:

In the intermediate complexity model Bern3D v2.0 a single layer energy-moisture balance atmosphere with a thermodynamic sea-ice component (Ritz *et al* 2011) is coupled to a 3D geostrophic-frictional balance ocean component (Edwards *et al* 1998, Müller *et al* 2006) with an isopycnal diffusion scheme and Gent-McWilliams parameterization for eddy-induced transport (Griffies 1998). Carbonate chemistry and air-sea gas exchange is implemented according to OCMIP-2 protocols (Najjar and Orr 1999, Orr *et al* 1999) with updates for the calculation of the Schmidt number (Wanninkhof 2014). The calculation of the carbonate chemistry is done with the mocsy 2.0 routine (detailed in Orr and Epitalon 2015) and calculates the carbonate species, and hence surface ocean pCO_2, from temperature, salinity, and concentrations of alkalinity and DIC at each time step. Marine primary productivity is restricted to the euphotic zone (75 m) and is calculated as a function of nutrient concentrations (P, Fe, Si), temperature and light availability (Parekh *et al* 2008, Tschumi *et al* 2011). Remineralization of organic matter at depth follows a Martin's Curve (Martin *et al* 1987) and in the case of $CaCO_3$ and opal takes place with an e-folding depth-scale of 5066 and 10 000 m, respectively. The model configuration does not include marine sediments. Coupled to the Bern3D is the land surface processes and eXchanges (LPX-Bern) model v1.5 (Lienert and Joos 2018). LPX-Bern is a dynamic global vegetation model and simulates the coupled cycles of nitrogen, water and carbon. Vegetation is represented by 20 plant functional types (15 on natural and 5 on anthropogenically used land) that compete within their bioclimatic limits for resources.

UVic-ESCM v2.10:

The UVic-ESCM v2.10 is an intermediate complexity model (Weaver *et al* 2001, Mengis *et al* 2020) with a three-dimensional ocean coupled to a two-dimensional energy moisture balance model of the atmosphere. The ocean component includes a representation of biogeochemistry (Schmittner *et al* 2005, Keller *et al* 2012) and a thermodynamic-dynamic sea ice model (Bitz *et al* 2001). The global carbon cycle is simulated with air-sea gas exchange of CO_2 and marine inorganic carbonate chemistry following OCMIP-2 protocols (Orr *et al* 1999) as described by Ewen *et al* (2004). Surface pCO_2 is calculated as a function of temperature, salinity, alkalinity, and DIC. The inorganic carbon cycle is coupled to a nutrient-phytoplankton-zooplankton-detritus marine ecosystem model (Keller *et al* 2012). Phytoplankton and zooplankton contributions to the inorganic carbon cycle (alkalinity and DIC tracers) are calculated from particulate organic carbon production and remineralization using a fixed rain ratio. The production of calcium carbonate is parameterized as a fixed ratio of the production of non-diazotrophic detritus (Keller *et al* 2012). The $CaCO_3$ produced then contributes to DIC and alkalinity with a fixed remineralization profile exponentially dependent on depth. The terrestrial component accounts for vegetation dynamics and incorporates five different plant functional types (Meissner *et al* 2003). Additionally, the model includes a representation of permafrost carbon (MacDougall and Knutti 2016).

2.2. Experimental setup and analysis

From a pre-industrial spin-up, the models are forced with historical CO_2 emissions (Friedlingstein *et al* 2020), non-CO_2 radiative forcing from other well-mixed greenhouse gases, and changes in radiative forcing from aerosols according to Dentener *et al* (2021). Historical land-use area changes (Hurtt *et al* 2019, 2020) as well as nitrogen deposition and fertilization of agricultural land (Hegglin *et al* 2016, Lu and Tian 2017, Xu *et al* 2019) are further prescribed to the LPX land component, while for the UVic-ESCM land component TRIFFID nitrogen deposition and fertilization is not prescribed.

From the historical run, future scenarios are branched off (see figure 1) and run until 2100 CE (UVic-ESCM) or 2300 CE (Bern3D-LPX). Emissions follow data from the SSP database (Riahi *et al* 2017), land-use forcing data from Hurtt *et al* (2020), and other forcing according to Dentener *et al* (2021). From the different scenarios, the SSP5-3.4 overshoot scenario (from hereon SSP5-3.4) is run once in its regular design and once with additional OAE. Under OAE, alkalinity is added uniformly to the ice-free surface ocean grid cells between 60° S and 70° N. OAE begins in the year 2025 CE and is linearly ramped up to its maximum value of 0.1375 Pmol yr^{-1} (0.135 in the case of UVic-ESCM) at the start of the year 2035 CE and constant thereafter. At the end of year 2220 CE, OAE is abruptly stopped and kept at zero thereafter.

In addition to the OAE experiment on top of SSP5-3.4, we conduct an idealized CO_3 peak-decline experiment with the Bern3D-LPX ensemble. In this experiment, atmospheric CO_2 is assumed to increase exponentially from the pre-industrial level of 276.58 ppm to 648 ppm within 116 years. Afterward, CO_2 declines at the same rate until stabilization at 431 ppm (figures 1(c) and 4(a)). This decline can be thought of as the result of any kind of CDR. The CO_2-forcing corresponds to a linear increase in radiative forcing to 4.5 Wm^{-2} and a decrease to 2.4 Wm^{-2} and was selected to result in a peak warming of 2 °C followed by a cooling to 1.5 °C when applying the Bern3D-LPX standard parameters.

Ensemble generation, sampled parameters, and calculation of ensemble member skill scores differ slightly between the two models. In the case of Bern3D-LPX, a 1000-member perturbed parameter ensemble was generated where 27 key model parameters were sampled using Latin Hypercube sampling (McKay *et al* 1979). The perturbed model parameters affect the diffusivities in atmosphere and ocean, atmosphere–ocean gas transfer, the radiative forcing from greenhouse gases and aerosols, terrestrial photosynthesis, hydrology, vegetation dynamics, soil organic matter decomposition, and turnover, as well as the nominal climate sensitivity of the model (see table 1 in the SI). The selection of parameters builds upon earlier work (Steinacher *et al* 2013, Steinacher and Joos 2016, Lienert and Joos 2018), by choosing the prior distributions of the parameters for this study according to constrained posterior distributions from the studies above.

In the case of UVic-ESCM, 18 model parameters were perturbed, representing important processes in all the main components of the model, i.e. atmospheric energy and moisture balance, climate sensitivity, ocean physics, ocean biogeochemistry, terrestrial biogeochemistry, and the cryosphere. The parameter selection builds upon previous works exploring model parametric uncertainty and sensitivity analysis (Goes *et al* 2010, Olson *et al* 2012, MacDougall and Knutti 2016, Mengis 2016, Ehlert *et al* 2017, Tran *et al* 2020). As the UVic-ESCM is more computationally expensive, running thousands of simulations to thoroughly explore the 18-dimension parameter space is not practical. Instead, we used Gaussian process emulation (Sacks *et al* 1989, Kennedy and O'Hagan 2001, Rasmussen and Williams 2006) in combination with history matching (Andrianakis *et al* 2015, Williamson *et al* 2017) to efficiently sample the inputs of interest and to serve as a statistical proxy for the full model. More details on sampled ranges of the parameters can be found in the Supplementary Information.

To reduce uncertainties, we exploit a broad set of observation-based data (SI figure 1 and SI tables 2 and 4) and constrain both model ensembles to realizations that are compatible with observations, thereby probing both, the mean state and the transient response in space and time of the ensemble members. The data set combines information from satellite, ship-based, ice-core, and in-situ measurements and includes estimates of SAT change, ocean heat uptake, seasonal and decadal atmospheric CO_2 change, and ocean and land carbon uptake rates, eight physical and biogeochemical three-dimensional ocean tracer fields, including carbon isotopes, as well as land carbon stocks, fluxes, and fraction of absorbed radiation.

3. Results

Mean projections for CO_2 and SAT change since pre-industrial (ΔSAT) agree between the two model systems within uncertainties (figure 1). Uncertainty estimates are similar for CO_2 but larger in ΔSAT for the constrained Bern3D-LPX ensemble than the constrained UVic-ESCM-emulator ensemble (right panels in figures 1(c) and (d)). The cumulative mean ocean uptake until 2100 CE across the different scenarios is larger by ~50–100 GtC in the Bern3D-LPX than in the UVic-ESCM ensemble. On the other hand, land biosphere uptake is ~50–100 GtC larger in UVic-ESCM than in Bern3D-LPX, leaving the total land-ocean sink more similar across the two model ensembles. Bern3D-LPX is known to feature a relatively weak terrestrial carbon sink in comparison to observational estimates (Lienert and Joos 2018).

With Bern3D-LPX, atmospheric CO_2 is projected to peak in the 21st century and approach values of 372 [362–380] and 363 [352–371] ppm towards 2300 CE under the two overshoot scenarios SSP1-2.6 and SSP5-3.4, respectively. Correspondingly, ΔSAT peaks at around 1.7 [1.4–2.0] and 2.2 [1.9–2.6] °C in the second half of the 21st century and approaches 1.1 [0.9–1.3] and 1.0 [0.8–1.3] °C towards 2300 CE in Bern3D-LPX under scenarios SSP1-2.6 and SSP5-3.4, respectively. With UVic-ESCM, ΔSAT peaks at 1.8 [1.6–2.0] and 2.3 [2.1–2.5] °C, and is also declining in SSP1-2.6 and SSP5-3.4 in 2100 CE, when the simulations end.

With massive OAE, CO_2 continues to decline, starts to increase slightly after OAE stoppage after 2220 CE, and reaches values of 320 [310–327] ppm in 2300 CE for SSP5-3.4 + OAE. The additional decline results from additional ocean C uptake, counteracted by increased carbon loss from the land biosphere (cf figures 1(e) and (f)). While CO_2 has reached values close to pre-industrial by 2300 CE (figure 1(c)), ΔSAT, is still elevated by 0.7 [0.5–0.8] °C by 2300 CE (figure 1(d)). Thus, global warming remains irreversible over many centuries even if massive OAE were feasible.

3.1. Changes and trade-offs in the global carbon sinks, atmospheric CO_2, and the efficiency of CDR

Under CDR, the ocean stores more carbon as a result of OAE. However, Earth system feedbacks linked to atmospheric CO_2 partly offset the direct alkalinity-driven ocean uptake. We use the symbol δ to denote the difference in carbon inventories between simulations with and without OAE.

In simulations with prescribed CO_2 and, thus, with suppressed feedback from δCO_2, δocean is quantified to 251 GtC (20.9 Pmol) in response to the addition of 26.26 Pmol of alkalinity until the end of the year 2220 CE for the standard parameter

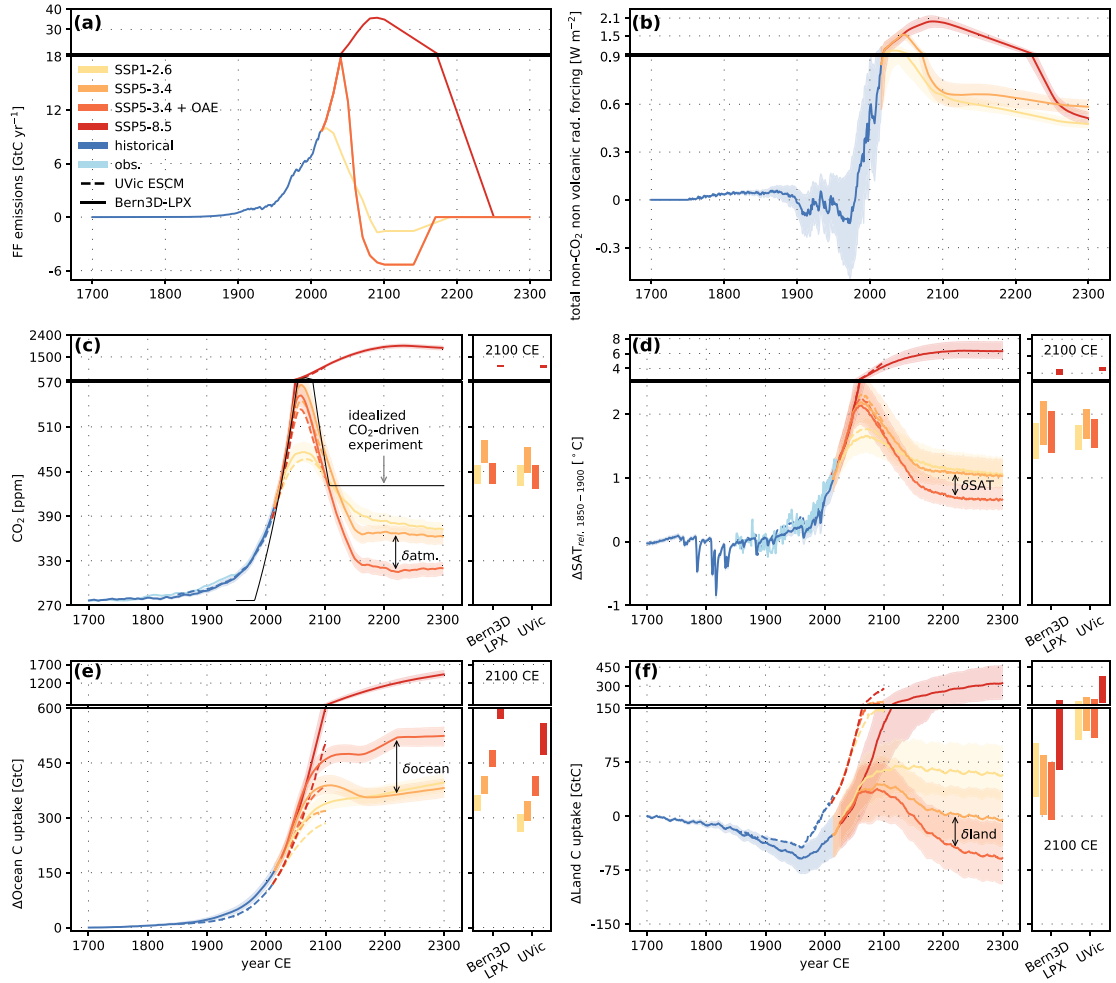

Figure 1. Time series of prescribed (a) fossil-fuel (FF) CO_2 emissions, (b) total non-CO_2 radiative forcing and simulated (c) atmospheric CO_2, (d) surface air temperature (SAT, relative to 1850–1900 CE), (e) cumulative atmosphere-ocean carbon flux, and (f) cumulative atmosphere-biosphere carbon flux. For the Bern3D-LPX model the skill-weighted mean (solid lines) and 68% confidence interval (c.i., shading) and for the UVic-ESCM model the skill-weighted mean (dashed lines) are shown. Black arrows indicate the difference (δ) between SSP5-3.4 with and without OAE. Panels on the right of subplots (c)–(f) show the 68% c.i. of the skill-weighted ensemble in the year 2100 CE. Cumulative carbon fluxes prior to 1850 (simulation start of the UVic-ESCM ensemble) of Bern3D-LPX have been added to UVic-ESCM data in panels (c) and (d). Forcing of SSP5-3.4 + OAE is the same as SSP5-3.4 without OAE in panels (a) and (b).

Bern3D-LPX ensemble member. The massive application of OAE would thus allow for an additional 251 GtC of emissions until 2220 CE while keeping CO_2 at the same level as without OAE.

We define the efficiency of alkalinization, $\varepsilon_{\delta\text{inventory}}$, as the ratio of δinventory per unit alkalinity added in mol (i.e. mol carbon per mol alkalinity, table 1). Then, for the ocean, $\varepsilon_{\delta\text{ocean}}$ is 0.8 mol mol^{-1} (20.9 Pmol/26.26 Pmol). The atmospheric CO_2 reduction (δatm) in the corresponding emission-driven (superscript e), δCO_2-feedback-enabled simulations with the full ensemble amounts to −111 [−118 to −103] GtC, equivalent to about −9.2 [−9.8 to −8.6] Pmol and −52 [−56 to −49] ppm CO_2 (figure 2(a)). The efficiency $\varepsilon^e_{\delta\text{atm}}$ is −0.35 [−0.37 to −0.33] mol mol^{-1}. Thus, taking the results from the Bern3D-LPX standard parameter member for comparison, the realized atmospheric CO_2 reduction, and correspondingly the efficiency, is more than 2 times smaller than the direct alkalinity-driven enhancement of ocean uptake. This muted atmospheric response to OAE is caused by a reduction in the ocean and land carbon sink due to the reduction in atmospheric CO_2. δland is −44 GtC [−55 to −32], i.e. lower land sink with than without OAE in the emission-driven simulations at the end of the year 2220 when OAE stops (figure 2(c)). δocean is 155 [146–162] GtC (figure 2(b)) and, thus, 96 GtC lower compared to the concentration-driven, δCO_2-feedback-disabled simulation with the standard parameter member. $\varepsilon^e_{\delta\text{ocean}}$ from the emission-driven runs is 0.49 [0.46–0.51] mol mol^{-1} in 2220 CE.

In conclusion, ~56% of the alkalinity-driven ocean uptake is offset by a reduction in the land and ocean sink due to lower CO_2 in the δCO_2-feedback-enabled simulations with freely evolving atmospheric CO_2 at the end of OAE in year 2220. Similar trade-offs hold for other CDR methods and vice-versa for

Table 1. Efficiency ($\varepsilon_{\delta\text{inventory}}$) of OAE for the ocean and atmosphere carbon reservoirs in concentration-driven (no CO_2-feedbacks) and emissions-driven (superscript e) simulations for the Bern3D-LPX and UVic-ESCM (where available). In the emission-driven case, skill-weighted mean and 68% c.i. are shown, while for the concentration-driven case, values from the standard parameter Bern3D-LPX ensemble member are reported.

	Year 2100 CE (mol C/mol alkalinity)		Year 2220 CE (mol C/mol alkalinity)
	Bern3D-LPX	UVic-ESCM	Bern3D-LPX
$\varepsilon^{e}_{\delta\text{atm}}$	−0.54 [−0.57 to −0.51]	−0.44 [−0.47 to −0.41]	−0.35 [−0.37 to −0.33]
$\varepsilon_{\delta\text{ocean}}$	0.82		0.81
$\varepsilon^{e}_{\delta\text{ocean}}$	0.62 [0.60–0.63]	0.60 [0.58–0.61]	0.49 [0.46–0.51]

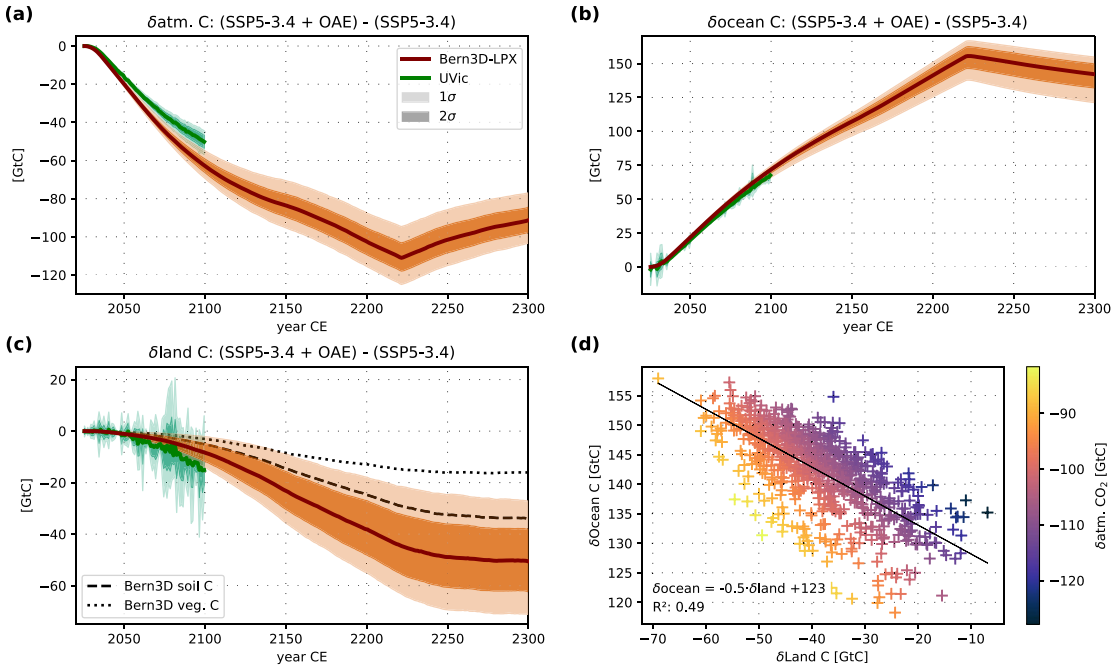

Figure 2. Potential impacts of ocean alkalinization on major carbon inventories. Timeseries illustrating the temporal evolution and ensemble spread ($\pm1\sigma$ and $\pm2\sigma$) in the (a) annual-mean atmospheric carbon inventory, the cumulative (b) air-sea, and (c) air-land carbon flux differences (δ) between [SSP5-3.4+OAE including artificial ocean alkalinization] minus [SSP5-3.4] for the Bern3D (orange) and UVic-ESCM (green) ensembles. (d) scatterplot summarizing mean changes (prior to OAE stoppage, 2190–2220) in the three carbon reservoirs for individual Bern3D ensemble members (crosses). Note in (c) also the skill-weighted mean response in the soil and vegetation carbon pool for Bern3D-LPX is shown (black dashed and dotted line).

positive emissions, where only a fraction accumulates in the atmosphere (airborne fraction). Although absolute numbers differ (table 1), the same behavior is apparent for the UVic-ESCM ensemble: an increased ocean carbon sink as a result of OAE is partly offset by reduced uptake/release of land carbon, leading to lower atm. CO_2 as compared to no OAE (figure 2).

The relationship between δland, δocean and δatm is visualized for individual Bern3D ensemble members at the end of OAE application (figure 2(d)). In general, there is a negative relationship between δocean and δland: the larger δocean, the larger δland carbon due to OAE. Largest reductions in atmospheric CO_2 (δatm) are achieved for large δocean in interplay with small δland sources.

3.2. Spatial patterns in carbon sinks

Next, we discuss where the carbon is stored which is taken out of the atmosphere under SSP5-3.4 (ΔC) and additionally in response to OAE (δC; SSP5-3.4+OAE minus SSP5-3.4). The simulated spatial pattern for the column inventory of ΔDIC (figures 3(a) and (b)) is similar to reconstructions of historical anthropogenic carbon uptake (Sabine *et al* 2004), with large inventories in the North Atlantic and Antarctic Intermediate Waters. The pattern of the OAE-driven DIC increase, δDIC, is similar to that of ΔDIC (figure 3) despite alkalinity being added uniformly to the ice-free surface ocean between 60° S and 70° N. Simulations with dye tracers and further analyses imply that the high δDIC column inventories in the Atlantic result primarily from circulation, causing a net transport of δDIC from the Indo-Pacific into the Atlantic, with modifications by carbon-climate feedbacks (see also Supplementary Information). On land, the pattern of changes in carbon storage under SSP5-3.4 is diverse and certain regions change from a carbon sink in 2069–2100 CE to a source in 2269–2300 CE (cf figures 3(a) and (b)). With OAE, the land

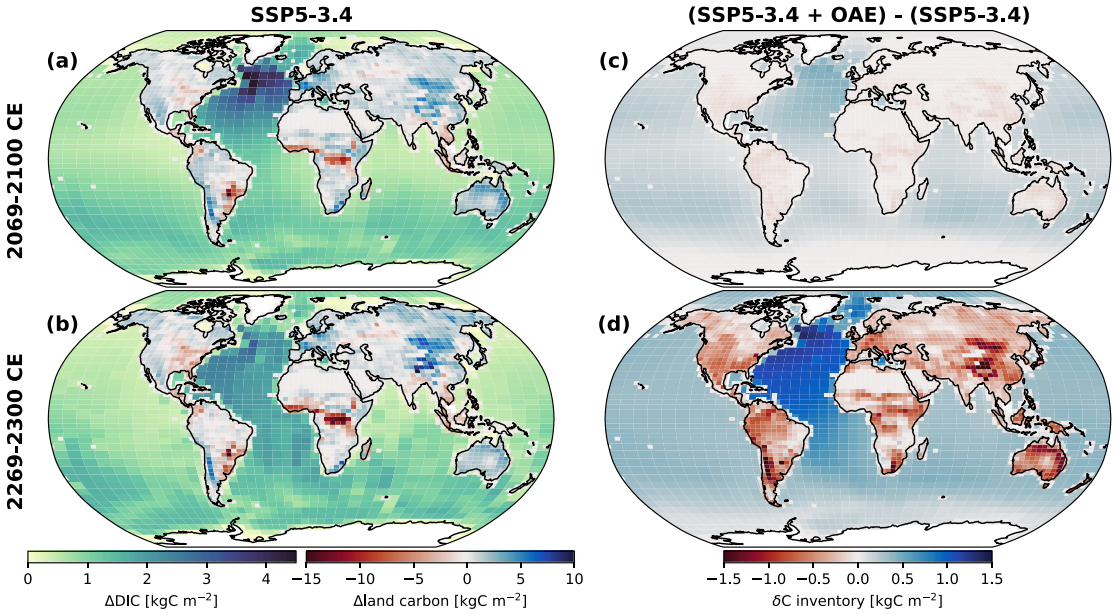

Figure 3. Skill-weighted mean changes (Δ) in ocean and land carbon inventory under SSP5-3.4 from the Bern3D-LPX for the period (a) 2069–2100 CE and (b) 2269–2300 CE relative to the 1850–1900 CE period as well as (c) and (d) the differences between SSP5-3.4 including ocean alkalinity enhancement (OAE) and SSP5-3.4 (δ) for the same periods.

biosphere loses carbon almost everywhere compared to SSP5-3.4 due to lower CO_2 (figures 3(c) and (d)).

3.3. Temporal lags in an idealized overshoot scenario

The question addressed in this section is to which extent climate change lags behind a decline in CO_2 achieved by a successful implementation of CDR. In other words, how long does it take for Earth system responses to manifest after the implementation of CDR. For illustration, we analyse the ΔSAT results from the idealized CO_2 peak-decline experiment conducted with the Bern3D-LPX model.

Earth system inertia causes ΔSAT to lag the decline in CO_2 (figures 4(a) and (b)). In response to the CO_2 forcing, ΔSAT peaks at 2.0 °C [1.8–2.3], declines afterward to a minimum of 1.3 °C [1.1–1.5] and slowly increases by about 0.1 °C [0.1–0.2] over the next 300 years under constant CO_2 and thus radiative forcing (figure 4(b)). Peak ΔSAT lags peak forcing by 5 [4–6] years and minimum ΔSAT is reached 47 [35–66] years after forcing has stabilized. Uncertainty in ΔSAT increases over time (purple shading in figure 4(b), as individual ensemble members reach their respective ΔSAT maximum/minimum at different times.

The temporal lag of the decline in ΔSAT behind the declining forcing is quantified following the schematic of figure 4(a). When CO_2 reaches 541 ppm (corresponding to 1.5 °C warming with the Bern3D-LPX standard parameter set), ΔSAT is 1.5 [1.3–1.7] °C during the warming phase at time t_1 but 1.8 [1.6–2.1] °C during the cooling phase at t_3. The additional time, τ_{lag}, required for ΔSAT to return to the value simulated at t_1 is 18 [14–22] years (figure 4(b)). τ_{lag} increases close to linearly with ECS (and consequently with TCR) and is around 20 years for an equilibrium climate sensitivity (ECS) of 3 °C (figure 4(c)). This relationship can be understood, simply put, as the more heat has accumulated (in the ocean), the longer it takes to get rid of this heat again. We conclude that inertia in the climate system causes the reduction in global warming to lag behind the implementation of CDR and the reduction in radiative forcing by several decades.

4. Discussion & summary

There are several implications from our study. First, the impact of CDR on atmospheric CO_2 will always be partly offset by subsequent weakened land and ocean carbon sinks, or even carbon losses, resulting in a muted atmospheric CO_2 reduction (e.g. Keller *et al* 2014, 2018a, González and Ilyina 2016, Jones *et al* 2016, Lenton *et al* 2018, Schwinger *et al* 2022). Here, we find in emission-driven simulations the effect of OAE on atmospheric CO_2 being partly offset by a loss of carbon from the land biosphere and a reduced marine carbon uptake in response to lower CO_2 with than without OAE. These responses in land and ocean uptake to OAE are in line with earlier studies (e.g. Keller *et al* 2014, González and Ilyina 2016, Lenton *et al* 2018), and further provide a longer perspective with simulations extending until 2300 CE, which seems important for the consideration of land biosphere effects (figure 1). A novel

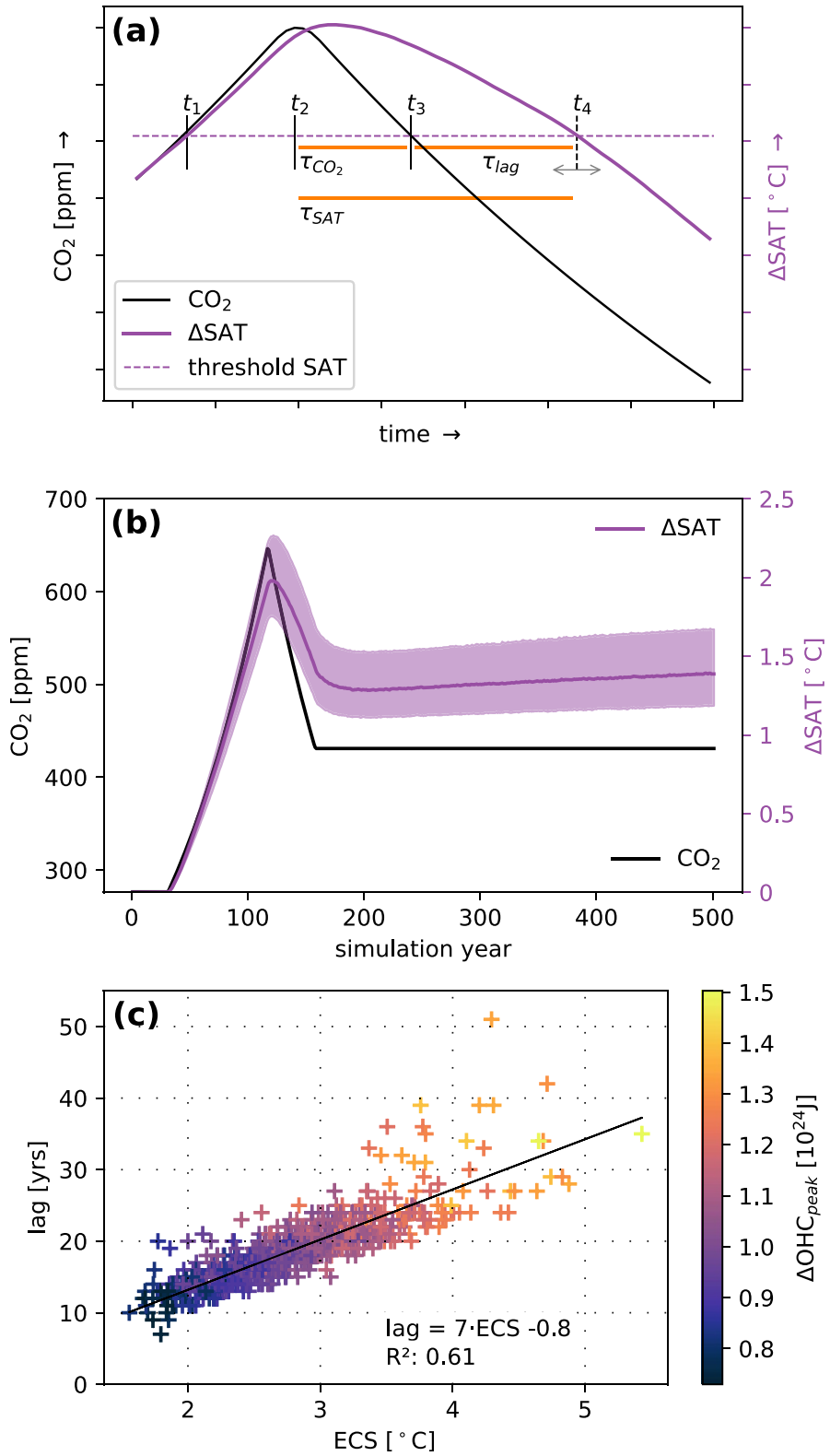

Figure 4. Idealized simulations to address temporal lags in overshoot scenarios. (a) Schematic how τ_{lag} is determined. Threshold ΔSAT is determined for each ensemble member at t_1, where $CO_2 = 541$ ppm (corresponding to 1.5 °C warming with the Bern3D-LPX standard parameter set). t_2 indicates the time at peak CO_2 and t_3 when CO_2 is the same as at t_1. t_4 is the time when ΔSAT reaches the threshold value and $\tau_{lag} = t_4$-t_3. (b) Temporal evolution of simulated ΔSAT (skill-weighted ensemble mean and 68% c.i.; purple line and shading, right y-axis) and prescribed CO_2 (black line, left y-axis). (c) Scatter plot of τ_{lag} vs. equilibrium climate sensitivity (ECS, see also the discussion) for individual ensemble members (crosses); colors show cumulative ocean heat uptake until peak CO_2 (ΔOHC_{peak}). Only ensemble members are included with ΔSAT reaching again the threshold value within an uncertainty of 0.1 °C.

finding of our study is that the efficiency of OAE, defined as mol ocean carbon uptake per mol alkalinity added to the ocean, is about 40% lower in emission-driven than concentration-driven simulations (table 1) and the atmospheric carbon inventory is reduced by only −0.35 [−0.37 to −0.33] mol C per mol alkalinity in the emission-driven Bern3D-LPX simulations. The atmospheric reduction by OAE is less than half of the direct alkalinity-driven enhancement of ocean uptake. Results from the UVic-ESCM-emulator ensemble, run until 2100 CE, support these findings. The same effects will hold for other ocean-based and vice versa for land-based CDRs (Oschlies 2009). The effectiveness of CDR in lowering atmospheric CO_2 (and thereby temperature) is therefore dependent on the response of the ocean and land biosphere to altered CO_2 and climate. The low efficiency of CDR in reducing atmospheric CO_2, as identified in this study, should arguably be considered when discussing the implementation of OAE and other CDR methods. Future research could investigate the efficiencies of a portfolio of simultaneous land- and ocean-based CDR applications.

Second, in overshoot scenarios, the timing of the peak, the decline, and the stabilization deviates between the forcing and the SAT response, leading to hysteresis (Boucher *et al* 2012, Zickfeld *et al* 2016). Hysteresis of SAT in the cumulative emission space has been shown to increase with higher ECS (Jeltsch-Thömmes *et al* 2020), while the lag, or lead, of maximum warming with respect to maximum forcing seems to depend on the zero emissions commitment, i.e. the warming, or cooling, after emission stoppage (Koven *et al* 2022, 2023). Joos *et al* (2013), based on 100 GtC pulse-release experiments, determined peak warming to lag the CO_2 emissions pulse by about 10 years. The lag results from an interplay of carbon cycle dynamics, climate sensitivity, and ocean thermal inertia and is influenced by the size of the emissions pulse (Zickfeld and Herrington 2015).

Here, using an idealized scenario, we find the response in ΔSAT to lag behind the declining forcing by about two decades (τ_{lag}: 18 [14–22] years) for a threshold temperature of around 1.5 °C (figure 4). The exact value of the lag depends on the scenario choice and the selected threshold. τ_{lag} increases ~linearly with ECS. The higher the ECS and thus the more heat has accumulated in the system, the larger τ_{lag} as it takes longer to get the excess heat out of the system (see figure 4(c)). This finding underlines the importance of considering uncertainties in our quantitative understanding of the Earth system reflected in the uncertainty of climate metrics such as, for example, the ECS.

There are limitations to our study. We apply Earth system models of intermediate complexity, in which many processes are highly parameterized. Examples include the remineralization of organic matter in the ocean or atmospheric heat and water fluxes following an energy-moisture balance.

For UVic, Gaussian Process emulation was applied to sample the 18-dimensional parameter space. An unavoidable trade-off exists between accuracy and efficiency as a result of using a fast statistical estimation to model the climate model's behaviour. The advantage of Gaussian Process emulation is that it provides an estimation of the uncertainty stemming from the emulator itself, and we take this uncertainty into account when computing the skill scores to weigh the ensemble (Supplementary Information). Another issue arising from the use of statistical estimation is that the quantities being emulated are not physically consistent, and therefore, mass conservation is not guaranteed. For instance, uncertainties in the emulated atmospheric, land, and ocean carbon budgets mean that the three terms do not necessarily sum to zero. Nevertheless, these simplifications and the low computational cost allow for large perturbed parameter ensembles, constraining these large ensembles with observational estimates, assigning skill scores to individual ensemble members, and enabling the calculation of probabilistic estimates of changes. For Bern3D-LPX, emulation was not needed and the 27-dimensional parameter space was explored with the coupled Bern3D-LPX.

Our application of OAE is idealized and neglects any barriers by assuming a linear increase in OAE capacity starting in 2025 CE up to a maximum deployment of 0.1375 Pmol yr^{-1} in 2035 CE. It is debatable, whether the amount of the maximum deployment is realistic at all (Köhler *et al* 2013), as it would mean mining, transporting, and distribution in the vast ocean ~5 Pg of an alkalizing agent such as $Ca(OH)_2$ (see Keller *et al* 2018b) every year. Fakhraee *et al* (2023) discuss in detail the attenuation of alkalinity release in the surface ocean through the removal (sinking) of particles prior to full dissolution. In their modeling study, they find that crystalline basalt and olivine release only <10% and ~50% of the alkalinity in the surface ocean (<80 m), respectively, while the effectiveness of alkalinity release is higher for artificial alkalizing agents such as MgO and CaO. Further, Fakhraee *et al* (2023) show a negative impact of olivine and basalt deployment on the marine biological pump based on their modeling study, while Ferderer *et al* (2022) find only moderate effects on various phytoplankton groups but a reduction in diatom biogenic silica buildup and silicic acid drawdown under OAE in microcosm studies. Another possible limitation of massive OAE relates to the secondary precipitation of $CaCO_3$ as a result of high alkalinity concentrations (Moras *et al* 2022, Hartmann *et al* 2023). The precipitation of $CaCO_3$ would reduce alkalinity and DIC in a 2:1 ratio, thereby shifting the acid-base balance towards higher CO_2 and, in turn, causing outgassing of CO_2 from the

surface ocean to the atmosphere (e.g. Sarmiento and Gruber 2006). Further, the applied OAE comes on top of CDR already included in the SSP5-3.4 scenario itself. However, the primary aim of this study is to investigate trade-offs in the carbon cycle and temporal lags under ocean-based CDR, putting the technical or societal feasibility of such an approach aside.

In summary, OAE leads to additional uptake of carbon by the ocean, thereby lowering atmospheric CO_2. This additional uptake from the atmosphere is partly offset by the release of carbon from the land biosphere and reduced ocean uptake under lower CO_2. Generally, the effectiveness of any CDR method in reducing atmospheric CO_2 and warming is muted by the response of the land and ocean carbon pools. In our study, we determine the efficiency of alkalinization in lowering atmospheric CO_2 to only around −0.35 mol C per mol alkalinity input. Even if large-scale OAE were technically feasible and accepted by the population, reducing CO_2 emissions to the extent possible remains urgent, because the efficiency of OAE, and other CDR methods, to lower atmospheric CO_2 is limited by tradeoffs between different carbon reservoirs and because changes in SAT lag behind the implementation of CDR and the decline in CO_2 forcing by decades.

Future research could focus on Earth system responses to a combination of different CDR approaches, likely needed to offset hard-to-abate residual emissions and reach net-zero carbon emissions.

Data availability statement

The data that support the findings of this study are openly available at the following URL/DOI: https://zenodo.org/doi/10.5281/zenodo.10040569 (Jeltsch-Thömmes *et al* 2023).

Acknowledgments

A J T, S L, and F J acknowledge funding from Swiss National Science Foundation (200020_200511) and all authors acknowledge the European Union's Horizon 2020 research and innovation programme under Grant Agreement No. 820989 (project COMFORT, Our common future ocean in the Earth system—quantifying coupled cycles of carbon, oxygen, and nutrients for determining and achieving safe operating spaces with respect to tipping points). D P K further acknowledges funding from the European Union's Horizon 2020 research and innovation programme under Grant Agreement No. 869357 (project OceanNETs). The work reflects only the authors' view; the European Commission and their executive agency are not responsible for any use that may be made of the information the work contains.

Calculations with the Bern3D-LPX model were performed on UBELIX (www.id.unibe.ch/hpc), the HPC cluster at the University of Bern.

Conflict of interest

The authors declare that they have no conflict of interest.

ORCID iDs

Aurich Jeltsch-Thömmes https://orcid.org/0000-0002-2050-1975
Giang Tran https://orcid.org/0000-0001-9815-3993
Sebastian Lienert https://orcid.org/0000-0003-1740-918X
David P Keller https://orcid.org/0000-0002-7546-4614
Andreas Oschlies https://orcid.org/0000-0002-8295-4013
Fortunat Joos https://orcid.org/0000-0002-9483-6030

References

Andrianakis I, Vernon I R, McCreesh N, McKinley T J, Oakley J E, Nsubuga R N, Goldstein M and White R G 2015 Bayesian history matching of complex infectious disease models using emulation: a tutorial and a case study on HIV in Uganda *PLoS Comput. Biol.* **11** e1003968

Battaglia G and Joos F 2018 Hazards of decreasing marine oxygen: the near-term and millennial-scale benefits of meeting the Paris climate targets *Earth Syst. Dyn.* **9** 797–816

Bitz C M, Holland M M, Weaver A J and Eby M 2001 Simulating the ice-thickness distribution in a coupled climate model *J. Geophys. Res.* **106** 2441–63

Boucher O, Halloran P R, Burke E J, Doutriaux-Boucher M, Jones C D, Lowe J, Ringer M A, Robertson E and Wu P 2012 Reversibility in an Earth system model in response to CO_2 concentration changes *Environ. Res. Lett.* **7** 024013

Burt D J, Fröb F and Ilyina T 2021 The sensitivity of the marine carbonate system to regional ocean alkalinity enhancement *Front. Clim.* **3** 624075

Campbell J S *et al* 2022 Geochemical negative emissions technologies: part I. Review *Front. Clim.* **4** 879133

Caserini S, Storni N and Grosso M 2022 The availability of limestone and other raw materials for ocean alkalinity enhancement *Glob. Biogeochem. Cycles* **36** e2021GB007246

Clark P U *et al* 2016 Consequences of twenty-first-century policy for multi-millennial climate and sea-level change *Nat. Clim. Change* **6** 1–10

Cooley S R, Klinsky S, Morrow D R and Satterfield T 2023 Sociotechnical considerations about ocean carbon dioxide removal *Annu. Rev. Mar. Sci.* **15** 41–66

Dentener F, Hall B and Smith C 2021 Annex III: Tables of historical and projected well-mixed greenhouse gas mixing ratios and effective radiative forcing of all climate forcers *Climate Change 2021: The Physical Science Basis. Contribution of Working Group I to the Sixth Assessment Report of the Intergovernmental Panel on Climate Change* ed V Masson-Delmotte *et al* (Cambridge University Press) pp 2139–52

Edwards N R, Willmott A J and Killworth P D 1998 On the role of topography and wind stress on the stability of the thermohaline circulation *J. Phys. Oceanogr.* **28** 756–78

Ehlert D, Zickfeld K, Eby M and Gillett N 2017 The sensitivity of the proportionality between temperature change and

cumulative CO_2 emissions to ocean mixing *J. Clim.* **30** 2921–35
Ewen T L, Weaver A J and Eby M 2004 Sensitivity of the inorganic ocean carbon cycle to future climate warming in the UVic coupled model *Atmos.-Ocean* **42** 23–42
Fakhraee M, Li Z, Planavsky N J and Reinhard C T 2023 A biogeochemical model of mineral-based ocean alkalinity enhancement: impacts on the biological pump and ocean carbon uptake *Environ. Res. Lett.* **18** 044047
Ferderer A, Chase Z, Kennedy F, Schulz K G and Bach L T 2022 Assessing the influence of ocean alkalinity enhancement on a coastal phytoplankton community *Biogeosciences* **19** 5375–99
Friedlingstein P *et al* 2020 Global carbon budget 2020 *Earth Syst. Sci. Data* **12** 3269–340
Frölicher T L and Joos F 2010 Reversible and irreversible impacts of greenhouse gas emissions in multi-century projections with the NCAR global coupled carbon cycle-climate model *Clim. Dyn.* **35** 1439–59
Fuss S *et al* 2018 Negative emissions-part 2: costs, potentials and side effects *Environ. Res. Lett.* **13** 063002
Goes M, Urban N M, Tonkonojenkov R, Haran M, Schmittner A and Keller K 2010 What is the skill of ocean tracers in reducing uncertainties about ocean diapycnal mixing and projections of the Atlantic Meridional Overturning Circulation? *J. Geophys. Res. Oceans* **115** 1–12
González M F and Ilyina T 2016 Impacts of artificial ocean alkalinization on the carbon cycle and climate in Earth system simulations *Geophys. Res. Lett.* **43** 6493–502
Griffies S M 1998 The Gent–McWilliams skew flux *J. Phys. Oceanogr.* **28** 831–41
Hartmann J, Jansen N, Dürr H H, Kempe S and Köhler P 2009 Global CO_2-consumption by chemical weathering: what is the contribution of highly active weathering regions? *Glob. Planet. Change* **69** 185–94
Hartmann J, Suitner N, Lim C, Schneider J, Marín-Samper L, Arístegui J, Renforth P, Taucher J and Riebesell U 2023 Stability of alkalinity in ocean alkalinity enhancement (OAE) approaches—consequences for durability of CO_2 storage *Biogeosciences* **20** 781–802
Hegglin M I, Kinnison D E and Lamarque J 2016 *CCMI Nitrogen Surface Fluxes in Support of CMIP6—Version 2.0, Edited* (Earth System Grid Federation)
Hurtt G C *et al* 2020 Harmonization of global land use change and management for the period 850–2100 (LUH2) for CMIP6 *Geosci. Model Dev.* **13** 5425–64
Hurtt G *et al* 2019 Harmonization of global land use change and management for the period 850–2015 (https://doi.org/10.22033/ESGF/input4MIPs.10454)
Ilyina T, Wolf-Gladrow D, Munhoven G and Heinze C 2013 Assessing the potential of calcium-based artificial ocean alkalinization to mitigate rising atmospheric CO_2 and ocean acidification *Geophys. Res. Lett.* **40** 5909–14
Jeltsch-Thömmes A, Stocker T F and Joos F 2020 Hysteresis of the Earth system under positive and negative CO_2 emissions *Environ. Res. Lett.* **15** 124026
Jeltsch-Thömmes A, Tran G, Lienert S, Keller D, Oschlies A and Joos F 2023 Model output from historical and future scenarios related to 'carbon dioxide removal: tradeoffs and lags' *Zenodo* https://doi.org/10.5281/zenodo.10040569
Jones C D *et al* 2016 Simulating the Earth system response to negative emissions *Environ. Res. Lett.* **11** 095012
Joos F *et al* 2013 Carbon dioxide and climate impulse response functions for the computation of greenhouse gas metrics: a multi-model analysis *Atmos. Chem. Phys.* **13** 2793–825
Keller D P, Feng E Y and Oschlies A 2014 Potential climate engineering effectiveness and side effects during a high carbon dioxide-emission scenario *Nat. Commun.* **5** 3304
Keller D P, Lenton A, Littleton E W, Oschlies A, Scott V and Vaughan N E 2018a The effects of carbon dioxide removal on the carbon cycle *Curr. Clim. Change Rep.* **4** 250–65
Keller D P, Lenton A, Scott V, Vaughan N E, Bauer N, Ji D, Jones C D, Kravitz B, Muri H and Zickfeld K 2018b The carbon dioxide removal model intercomparison project (CDRMIP): rationale and experimental protocol for CMIP6 *Geosci. Model Dev.* **11** 1133–60
Keller D P, Oschlies A and Eby M 2012 A new marine ecosystem model for the University of Victoria Earth system climate model *Geosci. Model Dev.* **5** 1195–220
Kennedy M C and O'Hagan A 2001 Bayesian calibration of computer models *J. R. Stat. Soc.* B **63** 425–64
Köhler P 2020 Anthropogenic CO_2 of high emission scenario compensated after 3500 years of ocean alkalinization with an annually constant dissolution of 5 Pg of olivine *Front. Clim.* **2** 575744
Köhler P, Abrams J F, Völker C, Hauck J and Wolf-Gladrow D A 2013 Geoengineering impact of open ocean dissolution of olivine on atmospheric CO_2, surface ocean pH and marine biology *Environ. Res. Lett.* **8** 014009
Koven C D *et al* 2022 Multi-century dynamics of the climate and carbon cycle under both high and net negative emissions scenarios *Earth Syst. Dyn.* **13** 885–909
Koven C D, Sanderson B M and Swann A L S 2023 Much of zero emissions commitment occurs before reaching net zero emissions *Environ. Res. Lett.* **18** 014017
Lenton A, Matear R J, Keller D P, Scott V and Vaughan N E 2018 Assessing carbon dioxide removal through global and regional ocean alkalinization under high and low emission pathways *Earth Syst. Dyn.* **9** 339–57
Lienert S and Joos F 2018 A Bayesian ensemble data assimilation to constrain model parameters and land-use carbon emissions *Biogeosciences* **15** 2909–30
Lu C and Tian H 2017 Global nitrogen and phosphorus fertilizer use for agriculture production in the past half century: shifted hot spots and nutrient imbalance *Earth Syst. Sci. Data* **9** 181–92
MacDougall A H 2013 Reversing climate warming by artificial atmospheric carbon-dioxide removal: can a Holocene-like climate be restored? *Geophys. Res. Lett.* **40** 5480–5
MacDougall A H and Knutti R 2016 Projecting the release of carbon from permafrost soils using a perturbed parameter ensemble modelling approach *Biogeosciences* **13** 2123–36
Martin J H, Knauer G A, Karl D M and Broenkow W W 1987 VERTEX: carbon cycling in the northeast Pacific *Deep Sea Res.* A **34** 267–85
McKay M, Beckman R and Canover W 1979 A comparison of three methods for selecting values of input variables in the analysis of output from a computer code *Technometrics* **21** 239–45
Meissner K J, Weaver A J, Matthews H D and Cox P M 2003 The role of land surface dynamics in glacial inception: a study with the UVic Earth System Model *Clim. Dyn.* **21** 515–37
Mengis N 2016 Towards a comprehensive, comparative assessment of climate engineering schemes metrics, indicators and uncertainties *PhD Thesis* Christian-Albrechts-University of Kiel
Mengis N *et al* 2020 Evaluation of the University of Victoria Earth system climate model version 2.10 (UVic ESCM 2.10) *Geosci. Model Dev.* **13** 4183–204
Minx J C *et al* 2018 Negative emissions—part 1: research landscape and synthesis *Environ. Res. Lett.* **13** 063001
Minx J C, Lamb W F, Callaghan M W, Bornmann L and Fuss S 2017 Fast growing research on negative emissions *Environ. Res. Lett.* **12** 035007
Moras C A, Bach L T, Cyronak T, Joannes-Boyau R and Schulz K G 2022 Ocean alkalinity enhancement—avoiding runaway $CaCO_3$ precipitation during quick and hydrated lime dissolution *Biogeosciences* **19** 3537–57
Müller S A, Joos F, Edwards N R and Stocker T F 2006 Water mass distribution and ventilation time scales in a cost-efficient, three-dimensional ocean model *J. Clim.* **19** 5479–99
Najjar R G and Orr J C 1999 Biotic-HOWTO. Internal OCMIP *Technical Report* (LSCE/CEA)

Olson R, Sriver R, Goes M, Urban N M, Matthews H D, Haran M and Keller K 2012 A climate sensitivity estimate using Bayesian fusion of instrumental observations and an Earth System model *J. Geophys. Res. Atmos.* **117** 1–11

Orr J C and Epitalon J-M 2015 Improved routines to model the ocean carbonate system: Mocsy 2.0 *Geosci. Model Dev.* **8** 485–99

Orr J C, Najjar R, Sabine C L and Joos F 1999 Abiotic-HOWTO. Internal OCMIP *Technical Report* (LSCE/CEA)

Oschlies A 2009 Impact of atmospheric and terrestrial CO_2 feedbacks on fertilization-induced marine carbon uptake *Biogeosciences* **6** 1603–13

Oschlies A 2021 A committed fourfold increase in ocean oxygen loss *Nat. Commun.* **12** 2307

Parekh P, Joos F and Müller S A 2008 A modeling assessment of the interplay between aeolian iron fluxes and iron-binding ligands in controlling carbon dioxide fluctuations during Antarctic warm events *Paleoceanography* **23** A4202

Rasmussen C E and Williams C K I 2006 *Gaussian Processes for Machine Learning* (MIT Press)

Renforth P and Henderson G 2017 Assessing ocean alkalinity for carbon sequestration *Rev. Geophys.* **55** 1–39

Riahi K *et al* 2017 The shared socioeconomic pathways and their energy, land use and greenhouse gas emissions implications: an overview *Glob. Environ. Change* **42** 153–68

Ritz S, Stocker T F and Joos F 2011 A coupled dynamical ocean-energy balance atmosphere model for paleoclimate studies *J. Clim.* **24** 349–75

Rogelj J *et al* 2018 Scenarios towards limiting global mean temperature increase below 1.5 degrees C *Nat. Clim. Change* **8** 325–32

Sabine C L *et al* 2004 The oceanic sink for anthropogenic CO_2 *Science* **305** 367–71

Sacks J, Welch W J, Mitchell T J and Wynn H P 1989 Design and analysis of computer experiments *Stat. Sci.* **4** 409–23

Sarmiento J L and Gruber N 2006 *Ocean Biogeochemical Dynamics* (Princeton University Press) p 503

Schmittner A, Oschlies A, Giraud X, Eby M and Simmons H L 2005 A global model of the marine ecosystem for long-term simulations: sensitivity to ocean mixing, buoyancy forcing, particle sinking and dissolved organic matter cycling *Glob. Biogeochem. Cycles* **19** 1–17

Schwinger J, Asaadi A, Steinert N J and Lee H 2022 Emit now, mitigate later? Earth system reversibility under overshoots of different magnitudes and durations *Earth Syst. Dyn.* **13** 1641–65

Siegenthaler U and Oeschger H 1978 Predicting future atmospheric carbon dioxide levels *Science* **199** 388–95

Smith P *et al* 2016 Biophysical and economic limits to negative CO_2 emissions *Nature Clim. Change* **6** 42–50

Steinacher M and Joos F 2016 Transient Earth system responses to cumulative carbon dioxide emissions: linearities, uncertainties and probabilities in an observation-constrained model ensemble *Biogeosciences* **13** 1071–103

Steinacher M, Joos F and Stocker T F 2013 Allowable carbon emissions lowered by multiple climate targets *Nature* **499** 197–201

Tokarska K B and Zickfeld K 2015 The effectiveness of net negative carbon dioxide emissions in reversing anthropogenic climate change *Environ. Res. Lett.* **10** 094013

Tokarska K B, Zickfeld K and Rogelj J 2019 Path independence of carbon budgets when meeting a stringent global mean temperature target after an overshoot *Earth's Future* **7** 1283–95

Tran G T, Oschlies A and Keller D P 2020 Comparative assessment of climate engineering scenarios in the presence of parametric uncertainty *J. Adv. Model. Earth Syst.* **12** e2019MS001787

Tschumi T, Joos F, Gehlen M and Heinze C 2011 Deep ocean ventilation, carbon isotopes, marine sedimentation and the deglacial CO_2 rise *Clim. Past* **7** 771–800

United Nations 2015 Paris Agreement (available at: http://unfccc.int/files/essential_background/convention/application/pdf/english_paris_agreement.pdf)

Wang H, Pilcher D J, Kearney K A, Cross J N, Shugart O M, Eisaman M D and Carter B R 2023 Simulated impact of ocean alkalinity enhancement on atmospheric CO_2 removal in the Bering sea *Earth's Future* **11** e2022EF002816

Wanninkhof R 2014 Relationship between wind speed and gas exchange over the ocean revisited *Limnol. Oceanogr. Methods* **12** 351–62

Weaver A J *et al* 2001 The UVic earth system climate model: model description, climatology and applications to past, present and future climates *Atmos.-Ocean* **39** 361–428

Williamson D B, Blaker A T and Sinha B 2017 Tuning without over-tuning: parametric uncertainty quantification for the NEMO ocean model *Geosci. Model Dev.* **10** 1789–816

Xu R, Tian H, Pan S, Dangal S R S, Chen J, Chang J, Lu Y, Skiba U M, Tubiello F N and Zhang B 2019 Increased nitrogen enrichment and shifted patterns in the world's grassland: 1860–2016 *Earth Syst. Sci. Data* **11** 175–87

Zickfeld K and Herrington T 2015 The time lag between a carbon dioxide emission and maximum warming increases with the size of the emission *Environ. Res. Lett.* **10** 031001

Zickfeld K, MacDougall A H and Matthews H D 2016 On the proportionality between global temperature change and cumulative CO_2 emissions during periods of net negative CO_2 emissions *Environ. Res. Lett.* **11** 055006